An Integrated Vision-Based System for Spacecraft Attitude and Topology Determination for Formation Flight Missions

Aaron Rogers, Kalle Anderson, Anna Mracek, Ray Zenick
AeroAstro, Inc.
12 Farnsworth Street, 4th Floor, Boston, MA 02210; (617)451-8630
aaron.rogers@aeroastro.com, kalle.anderson@aeroastro.com, anna.mracek@aeroastro.com,
ray.zenick@aeroastro.com

ABSTRACT: With the space industry's increasing focus upon multi-spacecraft formation flight missions, the ability to precisely determine system topology and the orientation of member spacecraft relative to both inertial space and each other is becoming a critical design requirement. Topology determination in satellite systems has traditionally made use of GPS or ground uplink position data for low Earth orbits, or, alternatively, inter-satellite ranging between all formation pairs. While these techniques work, they are not ideal for extension to interplanetary missions or to large fleets of decentralized, mixed-function spacecraft. The Vision-Based Attitude and Formation Determination System (VBAFDS) represents a novel solution to both the navigation and topology determination problems with an integrated approach that combines a miniature star tracker with a suite of robust processing algorithms. By combining a single range measurement with vision data to resolve complete system topology, the VBAFDS design represents a simple, resource-efficient solution that is not constrained to certain Earth orbits or formation geometries. In this paper, analysis and design of the VBAFDS integrated guidance, navigation and control (GN&C) technology will be discussed, including hardware requirements, algorithm development, and simulation results in the context of potential mission applications.

INTRODUCTION

To determine pointing and position vectors in both local and inertial coordinate frames, multi-spacecraft missions typically utilize separate attitude determination and formation metrology systems. For low Earth orbits (LEO), fleet position and geometry knowledge is almost exclusively achieved by using GPS data or ground uplink. In the absence of this information, inter-satellite ranging between all member elements (e.g., RF, optically) is required in order to determine the system topology shape, though processed data is not able to provide the formation's attitude.
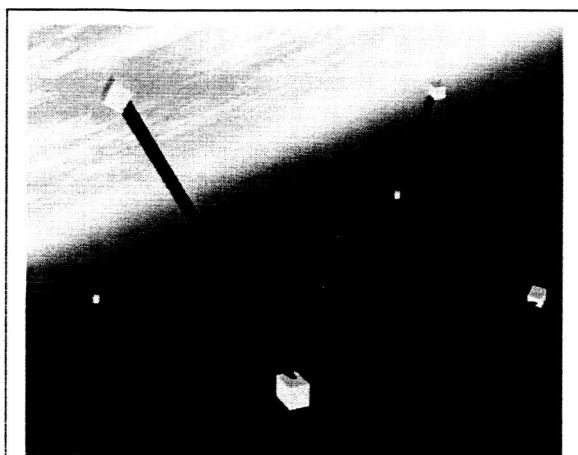

Figure 1: Multiple Spacecraft Operating in Formation through use of VBAFDS

While this works, NASA has established a priority for the deployment and coordination of large fleets of space platforms for missions that will span near-Earth and inter-planetary orbits [1]. Moreover, there are many scenarios in which one or more members of even a LEO mission may lack any or all external measurement data due to a particular orbit condition (e.g. Sun interference or ground uplink delays), or due to an onboard failure. To accommodate all these operational conditions, a navigation solution is required that is not reliant upon dedicated, expensive, and complex onboard systems, nor access to relative position knowledge solutions that constrain the formation to particular orbits and topologies.

The Vision-Based Attitude and Formation Determination System (VBAFDS) represents an integrated vision-based GN&C system technology for attitude and formation determination of multi-spacecraft missions. Figure 1 is a representation of a VBAFDS implementation in which member platforms are able to ascertain their formation topology through a minimal combination of vision and intersatellite-range data. To achieve this capability, the design will incorporate a novel miniature star tracker with a suite of innovative network algorithms. It will enable spacecraft attitude determination in inertial space, resolve the relative position of member elements of a formation flight mission or proximity operation, and accurately establish complete system geometry. Since it requires only a single node-node range measurement

and communication of processed vision data from member platforms, fleet geometry determination will be insensitive to orbit topology, near-field interference, and proximity. In order to preserve the advantages of an integrated solution, the VBAFDS design will be optimized around simplicity, cost, and efficient use of available platform resources.

This paper outlines preliminary design work that has been conducted by AeroAstro, Inc. under a Phase I Small Business Innovative Research (SBIR) contract to NASA GSFC. The requirements for the VBAFDS visual hardware system, algorithm development for star field analysis and formation determination, performance simulation tools, on board processing architecture, and candidate benchmark missions for VBAFDS implementation are discussed.

REQUIREMENTS DEFINITION FOR SPACECRAFT VISION HARDWARE

Star Tracker

In order to meet the desired mass and power requirements, the baseline VBAFDS design leverages a low-power, coarse star tracker that is currently in development by AeroAstro and the Massachusetts Institute of Technology Space Systems Laboratory [2]. The conceptual design for the AeroAstro Miniature Star Tracker (MST) features a simple lens to image stars of up to 4th magnitude onto a CMOS detector array, and a highly compact pattern recognition algorithm to find star pairs using a minimal catalog. The current design metrics for the MST system are outlined in Table 1.

The MST detector specifications are based in part on the FillFactory Image Sensors IBIS4 1.3 Mega Pixel CMOS APS Black and White detector [3], detailed in

Table 1: Miniature Star Tracker Design Objectives

Field of View	30 deg Conical
Accuracy	<100 arc-seconds, 3-σ
CMOS Imager	1000 x 1000 Pixel Array
Max Roll Rate	3.0 deg/sec
Update Rate	1 Hz
Mass	300 grams
Power	<1 W @ 5.5VDC
Dimensions	5.1 cm x 7.6 cm x 7.6 cm
Volume	300 cu cm
Output	Earth-Centered Inertial
Limiting Star Mag.	4th
Star Pairs Tracked Simultaneously	4 Max
Interface	RS-422
Radiation Tolerance	up to 20 Krad

Table 2.

Table 2: MST Detector Properties

Parameter	Value
Quantum Efficiency, η_{CCD}	0.60
Focal Length, FL	18 mm
Field of View, FOV	31°
Integration Time, t_{int}	10 ms
Number of Pixels	1000 x 1000
Array Dark Current, J_{dark}	344 pAmps/cm^2
Pixel Size	7 μm x 7 μm
Array Area, A_{Array}	1x10^{-6} m^2

As shown in Figure 2, with the stated specifications, MST functions under conditions of greater than 80% sky coverage, representing a very efficent, yet capable means of performing attitude determination. Exclusion angles for MST are approximately 50° and 25° for the Sun and Earth, respectively.
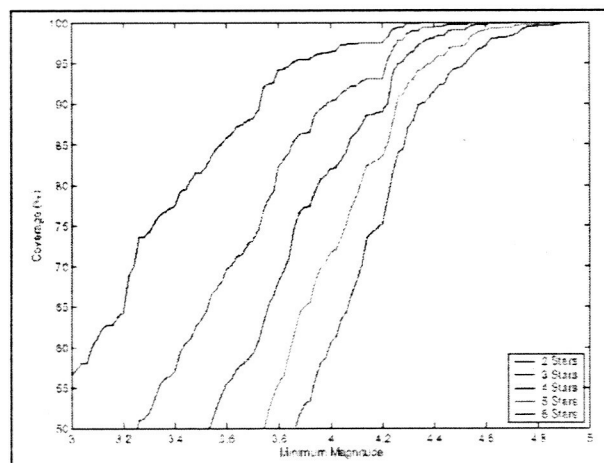

Figure 2: Approximate Sky Coverage by Minimum Magnitude for a 27.8deg FOV

Based upon the choice of detector, as shown in Figure 3, an experimentally verified relationship exists between required imager update frequency, for a given signal-to-noise ratio (SNR), and the limiting magnitude of observed star patterns.
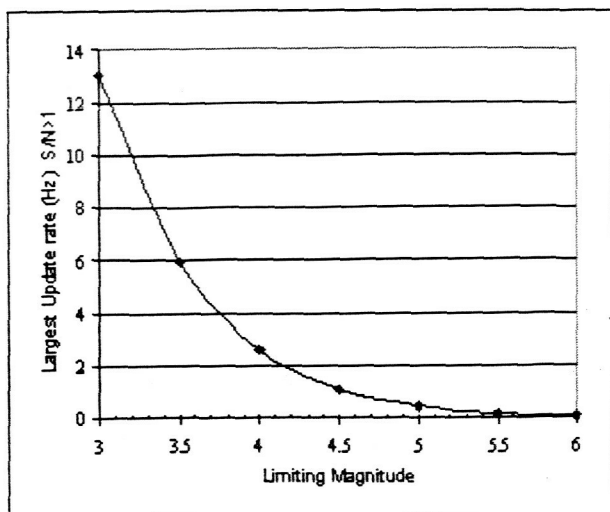
Figure 3: Update Rate vs. Limiting Magnitude

Based upon the trade-space associated with choices of array size and optical specifications, Table 3 details several alternate design configurations that have also been considered for VBAFDS.

Table 3: VBAFDS Candidate Imagers

Array Size (Pixels)	Pix Size (μm)	Angular Res/Pix (arc sec)	Focal Length (mm)	FOV Cone (deg)
1000 x 1000	10	114.6	18	31*
500 x 500	10	206	10	28
500 x 500	7.4	150	10	21
500 x 500	7.4	254	6	34
250 x 250	10	206	10	14
1000 x 1000	10	206	10	53

* Baseline MST configuration

Satellite Beacon

In order for member spacecraft of a formation to visually identify one another reliably, each must have its own light source. An analysis was conducted to assess the issues associated with utilizing a strobed beacon in conjunction with the MST detector. By incorporating the dispersion with separation distance and off-center viewing angles, required output power can be found as a function of baseline separation.

Foremost, the MST detector has a minimum required irradiance at the detector face of 1.16×10^{-9} W/m^2, corresponding to a minimum detectable photon flux of 3.45×10^9 photon/m^2/s. For a given beacon point source,

the effective irradiance reaching the detector was translated into a photon flux at the detector plane by using the rough approximation that all the photons were at the average energy for a photon of the peak wavelength λ. This photon flux was used with the optical and electrical properties of the detector to determine the output signal current resulting from the beacon. It was assumed that a beacon would appear as a point source, filling only one pixel in the detector. Possible spread effects were not included in this analysis.

The optical considerations were included through definition of an "effective pixel capture area," A_E, based on detector field of view (FOV) and focal length and normalized by the number of pixels in the array:

$$A_E = FL^2 \left(\frac{\Omega_C}{N_{Pixel}} \right) \tag{1}$$

where Ω_c is the solid angle resulting from the detector FOV. This step allows photon flux arriving from the light source, q, to be translated into a photon hit rate per pixel. The efficiency of the detector (η_{CCD}) can then be incorporated to resolve the signal current (J):

$$J = \eta_{CCD} \; q \; A_S \; e \tag{2}$$

where e is the charge on an electron.

Two components of detector noise were considered: photon noise and the array dark current associated with thermal noise. A Poisson distribution for photon noise was employed:

$$Noise_{Photon} = \eta_{CCD} \sqrt{q \; A_E} \tag{3}$$

The array dark current was normalized to give a value per pixel based on the total current output of the array and the sum of both of these error sources were used with the signal current calculated above to determine the SNR.

With these relationships in place, conclusions could be drawn about the beacon requirements as a function of baseline separation. By enforcing the minimum irradiance restriction, values for required beacon output power intensity(I_v) were obtained (Table 4). The resulting SNR at distances greater than 100m were, however, well within the noise of the detector. Instead, an SNR ≥ 1 was enforced, and new beacon requirements were determined (Figure 4).

Table 4: Beacon Requirements Based on Detector Sensitivity

Separation, $\theta v = 0°$	100m	1km	10km
Required I_V, [W/m^2]	0.0202	0.0404	2.162
Resulting SNR	1.53	0.115	0.0665
Separation, $\theta v = 23°$	**100m**	**1km**	**10km**
Required I_V, [W/m^2]	0.0202	0.0404	2.364
Resulting SNR	0.5	0.0076	0.0055

These results are generally applicable to any beacon light source. The dashed line represents requirements for an angular offset (θv) of 23°, while the solid line represents requirements for zero angular offset between the bore sight of the beacon and the center of the detector. The offset of 23° was determined by aligning the periphery angles of the beacon's beam and that of the detector's FOV, giving the maximum possible observance. While various light sources will have different beam angles, the fall-off with angular separation is still applicable to all cases. The maximum viewable angular separation will not be the same in all cases however.
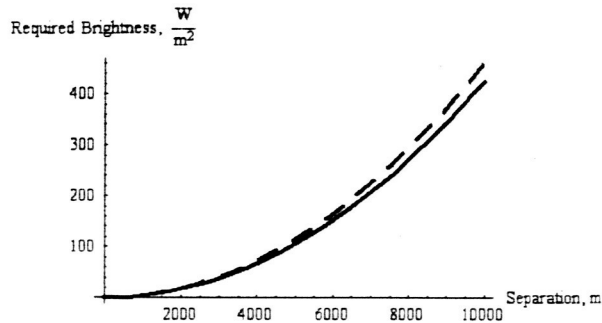
Figure 4: Required Beacon Brightness: 23° maximum angular offset (Dashed) and no offset (Solid)

These requirements were then applied to two candidate beacon light sources: an LED array and a standard industrial laser (Table 5).

Table 5: Typical Light Source Properties

Parameter	LED [4]	Laser [5]
Peak Wavelength, λ	592 nm	650 nm
Output Power, Iv	13800 mcd	3.5-4.0 mW
Forward Voltage	2.15 V	2.8-4.0 V
Forward Current	20 μA	50-65 mAmp
Diameter	5 mm	10.5mm
Beam Angle, θ	0.262 rad	1.3 mRad

The generic results of Figure 4 are interpreted using the LED specifications to generate Figure 5, which shows

the power that would be required to power a sufficiently bright LED beacon as a function of separation distance for both nominal and maximum-angular offset conditions.
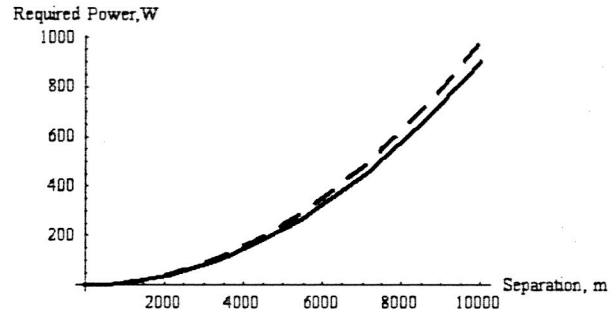
Figure 5: Required Power for LED Beacon: 23° maximum angular offset (Dashed) and no offset (Solid)

As can be seen, the power requirements for an LED beacon capable of meeting the brightness requirements at a satisfactory SNR with a MST-type detector, appear to be prohibitive at this stage. Conversely, the increased light output and lack of beam divergence available through use of a laser result in significantly lower predicted beacon power requirements. Based upon the worst-case forward voltage and current specifications, Figure 6 shows that the equivalent of an 8-laser cluster would be necessary to meet the irradiance and SNR requirements for the detector at 10km. This would draw a total of approximately 2W.
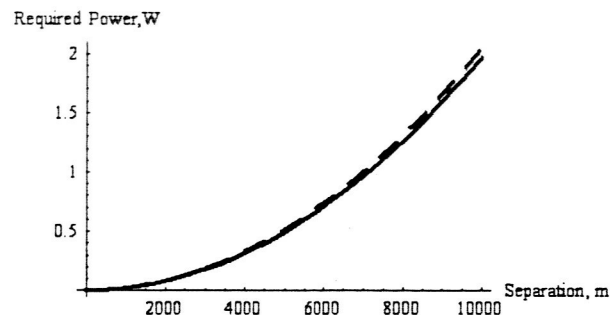
Figure 6: Required Power for Laser Beacon: 23° maximum angular offset (Dashed) and no offset (Solid)

From this preliminary analysis, one can see that the SNR is the driving factor in determining the required beacon light output. Thus it is especially important to realize that the detector specifications that were employed may be subject to correction or refinement as the design process progresses. Regardless of the

detector specifications, however, there is a significant power benefit to be obtained through the use of a laser light source. The tradeoff here is the reduction in observable angular separation. Using a laser limits the maximum visible angular separation to one half the FOV of the detector while the more diffuse LED beacon provides a contribution in the form of half the beam angle. Subsequent work will involve investigation of other possible light sources, such as high intensity LumiLEDs, Laser Diodes, and Laser LEDs.

ALGORITHM DEVELOPMENT

Attitude Determination in the Presence of Star Field Clutter

In order to use a Star Tracker for formation determination, the associated pattern matching software must be modified to recognize non-star objects as well as regular stars. This concept is illustrated in Figure 7.

Many well-documented star tracker algorithms specifically address the concept of 'false stars' in the context of radiation hits or reflections from debris that appear to be real stars. The Pyramid algorithm, developed by Junkins and Mortari [5], enables determination of an attitude solution with only 4 real stars in the presence of 24 false stars. The star tracker destined for the Rosetta Comet exploration mission is expected to track stars within the presence of thousands of false stars caused by reflections off of comet dust

particles [12]. The confidence that a positive star match can be made strictly depends upon how many real stars are visible and the probability that the false stars will take the shape of an actual constellation.
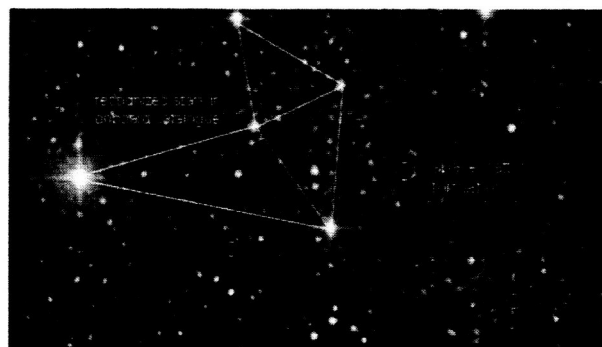

Figure 7: Sample Star Field as Seen by VBAFDS Imager with other Spacecraft in FOV

Once a star pattern match has been made with a small set of stars, the star tracker can compare the remaining objects in its field of view to its star catalog, using the computed attitude. Of the objects not matching the catalog, VBAFDS will need to differentiate between spacecraft beacons and other sources of false stars. Proton hits can be filtered by comparing several sequential image frames. Additionally, the member spacecraft beacons could be modulated with a recognizable sequence. Finally, there may be other ways to create a beacon such that it does not appear similar to actual stars. For instance, the point spread
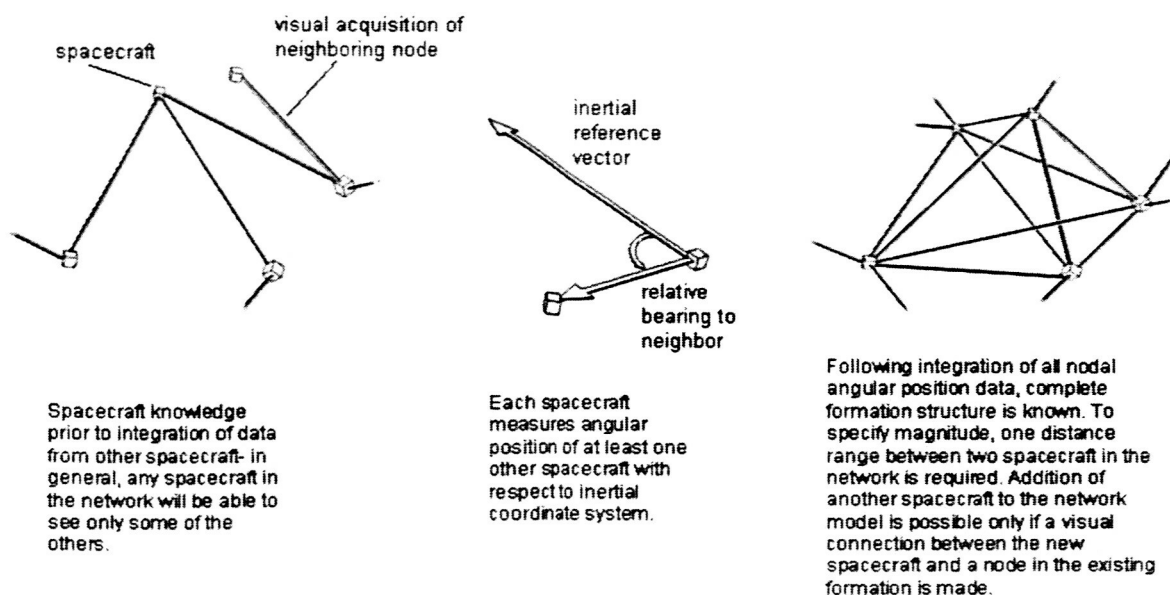

visual acquisition of neighboring node

spacecraft

inertial reference vector

relative bearing to neighbor

Spacecraft knowledge prior to integration of data from other spacecraft- in general, any spacecraft in the network will be able to see only some of the others.

Each spacecraft measures angular position of at least one other spacecraft with respect to inertial coordinate system.

Following integration of all nodal angular position data, complete formation structure is known. To specify magnitude, one distance range between two spacecraft in the network is required. Addition of another spacecraft to the network model is possible only if a visual connection between the new spacecraft and a node in the existing formation is made.

Figure 7: Methodology for Formation Topology Determination with VBAFDS

function of the beacon may appear different because the light will not be as collimated as starlight. Alternatively, two sets of optics share one detector. The first set of optics would pass all visible light to the detector, where the secondary set would have a narrow filter centered around the wavelength of the beacons and could purposefully add some identifiable aberration to the image. In this manner the beacon images would be optically tagged in the star field image. This is similar to an idea used on the StarNav II star tracker to image multiple fields of view on a single detector [6]. Once members of the formation have been identified, standard centroid-finding techniques will be used to compute relative bearing angles. Figure 7 illustrates the general VBAFDS methodology for determining a satellite formation geometry based on visual observation.

Determination of Formation Geometry

The VBAFDS algorithms are partitioned into two sections. The first component deals with determination of the relative positions of satellites in a constellation using a minimum set of measurements. The second element is concerned with incorporating additional measurements, measurement models, and dynamics models, to reduce the effects of random measurement error.

Geometry

The VBAFDS system produces two types of measurements: inter-satellite ranges and bearing angles between satellites. To produce an initial guess of the relative positions of satellites in the constellation, one satellite is picked as an arbitrary starting point. A range and bearing measurement to a second satellite will allow its position to be determined relative to the first satellite. This is continued until the position of all the satellites in the constellation have been referenced to each other.
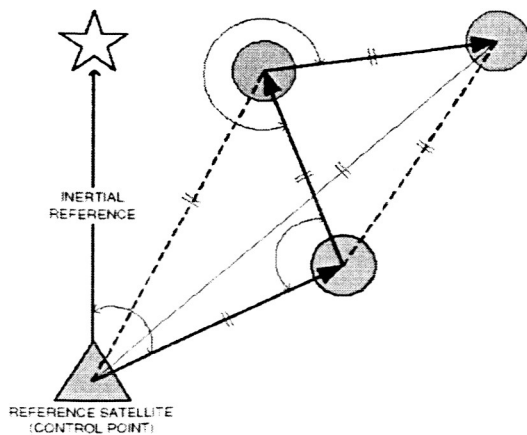

Figure 8: Satellite Referencing Schematic

The easiest case is when each satellite can be linked to another satellite via a range and bearing measurement. This type of arrangement forms a "traverse network" as shown in Figure 8. This figure shows a 2-D traverse network, but the concept can be easily extended to 3-D also. If some satellites are missing range or bearing measurements, then alternate solutions can be found using trilateration and triangulation, or intersection and resection, as shown Figure 9.

In such cases, the algorithm will first attempt to solve for positions for all the satellites connected by a traverse network. Then, the algorithm will attempt to use trilateration or triangulation to solve for the remaining unknown positions. With trilateration, if ranges are known to 3 other satellites, then the position of the fourth satellite can be found without any bearing information. This is similar to how GPS works. On the other hand, if only bearing angles to known positions are known, then triangulation can be used to solve for position.

Least-Squares

The previous section dealt with solving for an initial estimate of the relative positions of satellites in the constellation or formation. The process of forming that estimate incorporated the minimum number of observations possible. This second section of the VBAFDS algorithm deals with incorporating redundant observations, measurement models, and dynamics models to find a more optimal estimate of spacecraft positions.
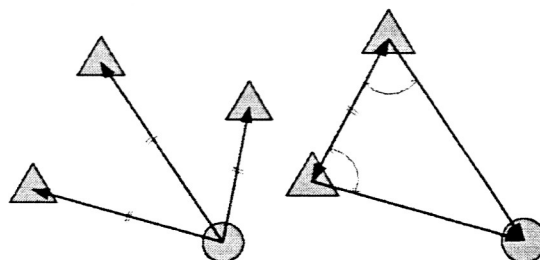

Figure 9: Triangulation Schematic

VBAFDS will employ algorithms commonly used in the fields of surveying and photogrammetry to solve for optimal position estimates, in the least-squares sense. Such algorithms combine redundant observations to find the optimal unknown variables that reduce the overall least-squares error. In the field of surveying, least-squares adjustment is the term applied to adjusting a set of observations to reduce overall error. In Photogrammetry, the term "Bundle Adjustment" is applied to the problem of jointly solving for optimal viewing structure and 3-D parameters.

$$\begin{bmatrix} \frac{\partial F_1}{\partial x_1} & \frac{\partial F_1}{\partial x_2} & \cdots & \frac{\partial F_1}{\partial x_n} \\ \frac{\partial F_2}{\partial x_1} & \frac{\partial F_2}{\partial x_2} & \cdots & \frac{\partial F_2}{\partial x_n} \\ \cdots & \cdots & \cdots & \cdots \\ \frac{\partial F_m}{\partial x_1} & \frac{\partial F_1}{\partial x_2} & \cdots & \frac{\partial F_1}{\partial x_n} \end{bmatrix} \begin{bmatrix} dx_1 \\ dx_2 \\ \cdots \\ dx_n \end{bmatrix} = \begin{bmatrix} l_1 - F_1(x_{1_0}, x_{2_0}, \ldots, x_{n_0}) \\ l_2 - F_2(x_{1_0}, x_{2_0}, \ldots, x_{n_0}) \\ \cdots \\ l_m - F_m(x_{1_0}, x_{2_0}, \ldots, x_{n_0}) \end{bmatrix} \begin{bmatrix} v_1 \\ v_2 \\ \cdots \\ v_m \end{bmatrix} \quad (4)$$

The expanded form of the standard Gauss-Newton least-squares adjustment: J X = K + V, is given in equation (4).

In this equation, the K matrix relates the residuals of the estimation procedure in which the F functions are measurement models that relate the current state estimate to observations that were made (the L vector). Solving for X produces a set of adjustments that can be added to the initial state estimate to reduce the least-squares error. Each observation can also be combined with a weighting function (W), to condition its use depending on accuracy:

$$X = (J^T W J)^{-1} J^T W K \quad (5)$$

The VBAFDS system will produce two types of measurements: range and bearing. Bearing could be represented in a number of forms, but for demonstration purposes it will be represented by an azimuth and elevation angle. Thus, there will be 3 measurement model equations. Each measurement model equation will take 2 three-dimensional positions as input, and compute the expected measurement given the current state estimate.

Given these measurement models, the $WJX = WK + V$, system of equations can be formed and the optimal least-squares solution can be found.

SIMULATION AND ESTIMATION OF PERFORMANCE

To aid in understanding the dynamics of the VBAFDS system, a six-degree-of-freedom (6DOF) numeric simulation environment has been developed. The simulation environment is written in C++, but has a flexible scripting interface using an open-source application extension language called Lua [16]. Additionally, the simulation provides three-dimensional visualization using OpenGL and the open-source scene graph library OpenSceneGraph.

Dynamics Models
The simulation environment models both orbital and attitude dynamics. The orbital dynamics model incorporates a J4 gravity model and allows for other perturbations such as drag or solar pressure to be added

in the future. The attitude dynamics model uses the Euler equations for rigid-body dynamics, where external effects on a body, such as forces and torques, can all be defined in the scripting interface. This flexibility enables ready simulation of different types of orbits and missions.

Visualization
One of the key problems for VBAFDS is whether or not satellites will be able to see other satellites. This is tied heavily to the VBAFDS FOV, the spin rate of the satellite (if any), and the type of orbit they are in. To aid in investigating these areas, the simulation has been equipped with rudimentary visualization capabilities which show how the member satellites move in relation to each other throughout their orbits, and how this affects their visibility from other member platforms.

The basic visualization system is driven through the Lua scripting interface. Models of satellites can be loaded into objects that can be positioned using the state vector variables from the dynamic simulation.

A screenshot from the simulation visualization is shown in Figure 10. A representative 30° field of view cone is projected from each satellite in the direction of its field of view. In this particular simulation, three of the satellites were initially oriented to face the fourth member of a formation. Colored cones corresponding to the VBAFDS FOV for each of the spacecraft are shown, with intensity varying depending on visibility conditions of other member satellites. When the fourth satellite is not visible, for example, the FOV cone is
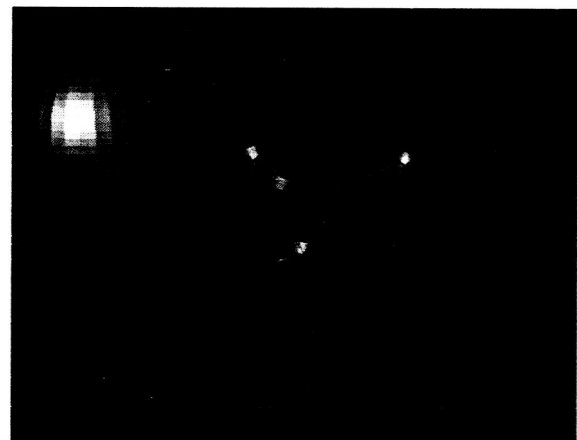

Figure 10: Simulation Frame - 4th Satellite Visible to Two of Three Others
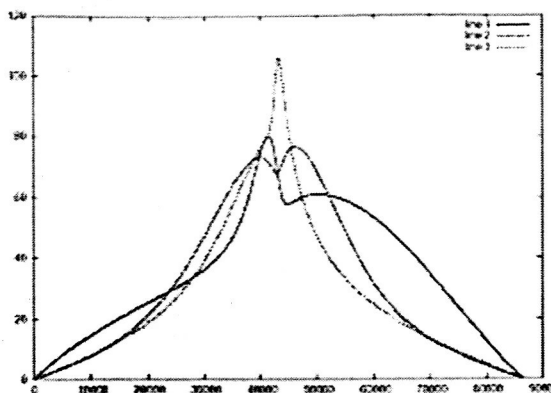
Figure 11: Variation of Net Bearing Angles

shown in a blue color. In the figure, the Earth is shown, as well as grey lines in the background that relate to the speed and direction of travel of the satellites relative to the observer.

For the depicted simulation, each satellite in the formation remained inertially pointed throughout the

orbit. The initial attitude of each element was set such that the bearing angle to the target spacecraft would be zero at the apogee of the orbit. The "net bearing angle" between two satellites is defined as the angle between the vector along the VBAFDS boresight and the vector between the two Centers of Mass (CM). Figure 11 shows how the net bearing angles vary over time for each satellite for this example. This type of graph enables estimates of system visibility conditions in which VBAFDS could make visual measurements. As such, a Monte Carlo analysis would provide information regarding optimized VBAFDS aperture orientation.

Based upon this access to relative bearing data generated by MST in conjunction with attitude determinatoin operations, and communicated range measurements between formation members (1m accuracy, 3σ), complete system topology in inertial space can be resolved. As shown in Figure 12, VBAFDS is also able to markedly reduce the overall variance of the position estimates by incorporating the redundant measurements.
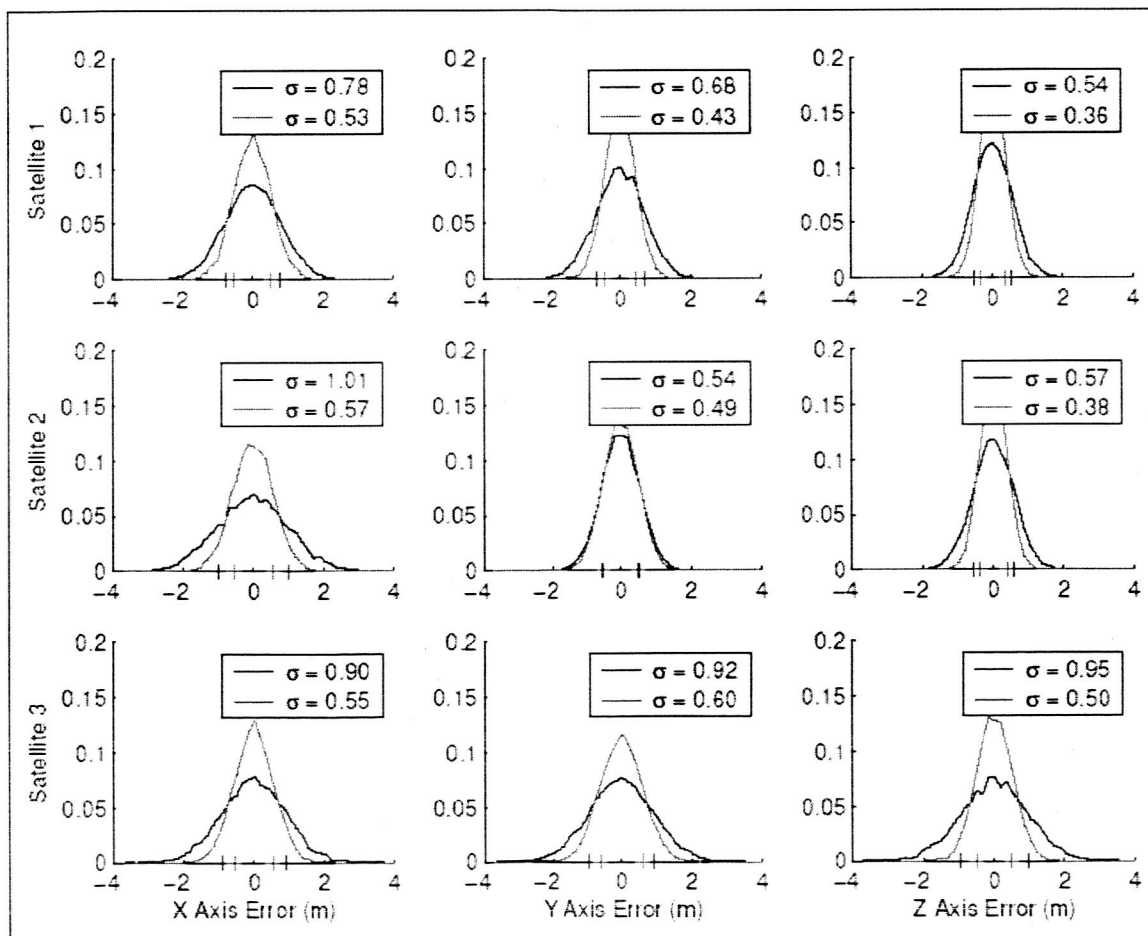

Figure 12: Estimated Position Error Distribution Before and After Least-Squares Adjustment

For missions utilizing spin-stabilized spacecraft, it is believed that the baseline VBAFDS design can accommodate angular rates of 2-3 RPM, with the potential to support as fast as 20 RPM through incorporation of electronic image "unwrapping" features that blend input from the spacecraft's angular rate sensors (in an IMU) and additional processing logic. It is recognized that despite the issues associated with accommodating attitude and formation determination under nominal body rotation, additional visual access to the formation may be realized.

PROCESSING ARCHITECTURE

VBAFDS operation is predicated upon effective utilization of measurement data, which may include GPS or TDRSS, for example, in addition to available intersatellite-range data. The concept of determining range data from a radio communications device is heavily dependent on the system clock stability, especially for small error, high accuracy, repeatable ranging measurements. These options vary in Allan Deviation from 1E-9/second stability, to 3E-13/second. Clock stability is not the only factor, however, due to several other parameters that will add significant error into the system's ranging calculations. These include fixed hardware delays, variable processor delays, and the kinematic stability of the reference datum being measured.

The ranging process includes:
- transmission of a range request by the launching terminal
- signal propagation
- remote terminal (N1) reception
- detection and processing
- retransmission
- return propagation and final reception
- processing of the return range data at the launching terminal (N0)

Note that the preprocessing time prior to initial request is excluded because it is not a critical part of the full timing cycle for the ranging process. Moreover, each of the time markers has an associated error. Understanding the source of these errors and estimating the quantitative impact on the range calculations is key to developing an accurate and repeatable ranging transponder system that is consistent with VBAFDS. A schematic of the overall VBAFDS processing architecture is shown in Figure 13.

REPRESENTATIVE MISSION SCENARIOS AND REQUIREMENTS

The Vision-Based Attitude and Formation Determination System is designed for use on any
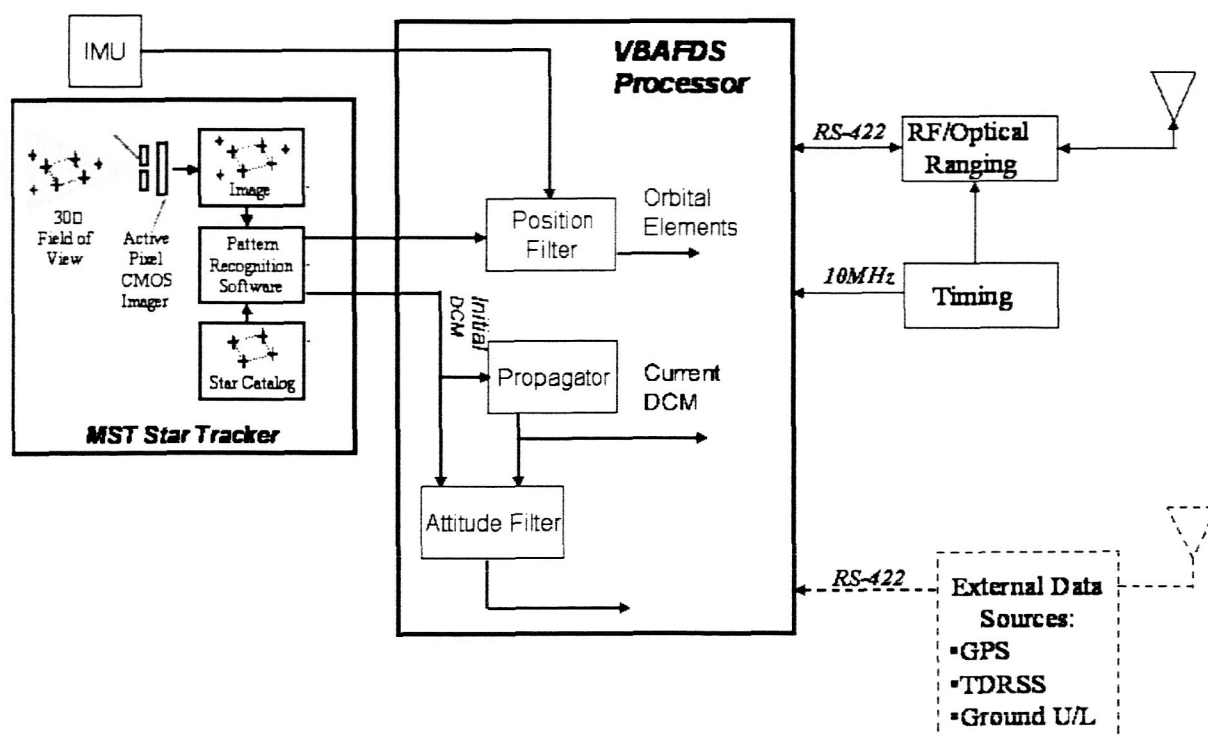

Figure 13: VBAFDS Processing Architecture

mission where spacecraft require knowledge of their positions relative to one another. As the primary missions of interest involve proximity operations or distributed spacecraft operations, a survey of proposed and operational missions was undertaken to identify characteristic geometries of interest. This led to a general, qualitative description of formation flight geometries, as well as more detailed descriptions of particular missions of interest. The four classifications of formation are listed below. It is worth noting here that Alfriend et al [13] has pointed out that formation flight missions unfailingly require much higher relative position accuracy than absolute position accuracy.

- In-plane (leader- follower): The formation spacecraft follow one another at close range in an identical orbit plane, i.e., "A-Train" and GRACE.

- Multi-plane: Spacecraft orbit in close proximity, not necessarily in identical orbit or in-plane, i.e., AURA, "Cluster" formation (ESA) and Magnetospheric Multiscale (MMS).

- Asymmetric in-plane constellation: Spacecraft are distributed throughout one orbital plane, with varying apogees and/or perigees, i.e., Magnetospheric Constellation (MagCon).

- Symmetric in-plane constellation: Spacecraft are distributed symmetrically along one or multiple identical planes, each of which is separated by right ascension of ascending node, i.e., Globalstar, Iridium, and Orbcomm.

- Operations outside Earth orbit: Spacecraft are operated at altitudes well beyond those continuously

served by terrestrial, LEO, or GEO resources, such as those involving lunar or libration point operations, i.e. Stellar Imager, Constellation-X, and MAXIM.

While these existing and proposed missions were categorized according to physically intuitive classifications and are not exhaustive of the possibilities, there are other ways of grouping missions. Sabol, et al [15], categorize formation flight geometries mathematically in terms of particular solutions to Hill's (Clohessy-Wiltshire) equations for relative motion between spacecraft, and the initial conditions which specify different flight geometries. Simplest among these is the "in-plane" formation, consisting of a number of spacecraft orbiting in the same plane, and separated only by mean anomaly. The "in-track" formation uses a small differential in the right ascension of orbital planes to permit the spacecraft to have identical ground tracks despite the rotation of the Earth.

A "circular" formation makes use of differences in inclination, RAAN, argument of perigee, and mean anomaly to maintain a constant distance between spacecraft throughout the orbit. The "projected circular" orbit also allows spacecraft to maintain constant distances from one another, but only in the along-track/cross-track plane. Sabol's "in-plane" formation is identical with that presented here, while their "in-track", "circular", and "projected circular" orbits all fall into the "multi-plane" category described here.

In conjunction with identified NASA priorities, Carpenter, et al [14], describes three reference mission classifications, detailed in Table 6. The baseline

Table 6: Applicable Mission Profiles (Reference Orbits)

Mission	Low Earth Orbit	Highly Elliptic Orbit	Libration Point
Apogee alt (km)	400	108 426	[transverse amplitude about L2 = 300 000]
Perigee alt (km)	400	1 276	[normal amplitude about L2 ≤ transverse amp.]
Inclination (deg)	97.03	5	-
Number of SC	6	4	20+
SC control	3-axis	Spin	3-axis
Relative position control requirement (m)	5 (with respect to desired relative trajectory)	10% of SC separation at apogee	0.01 (science mode)
Formation Topology	projected circular	tetrahedral	Aspherical
Pointing requirement (arcsec)	360	3600	1 (science mode)
Mission duration (yr)	2	2	12

VBAFDS design will support all of the discussed applications with the exception of the libration point mission. This mission has very high pointing accuracy requirements characteristic of astronomical interferometry that would likely preclude the use of VBAFDS as the primary means for performing attitude determination for such a mission, although use of an alternate imager could certainly enable this capability. Similarly, for missions with extremely long baseline separations, detector accuracy will govern relative position estimate error as a function of approximately 5E-6 units of baseline separation distance per arc-second of star tracker accuracy.

FUTURE WORK AND POTENTIAL APPLICATIONS

Future technical activities include the finalization of a formation determination algorithm set, optical and processing architecture specifications, and simulation and performance estimation. While the basics of the least-squares adjustment algorithms and how they are incorporated into the VBAFDS problem have been defined, the geometry solving algorithms, which use traverse networks, triangulation, and dilatation to find an initial state estimate, need to be formalized. In addition, further investigation will be done to define constraint equations and methods for blending various measurement data and propagating state estimates across periods of data drop-out.

In conjunction, the basic groundwork for a flexible simulation environment, which has been developed, will be extended to include models of the VBAFDS sensors. Ranging and bearing angle measurement models will be created which will accept the current state vector of the system as inputs in order to produce simulated measurement values as outputs, properly conditioned with noise. Additionally, the bearing angle model will only produce valid results when a satellite is in the simulated field of view. The outputs of these models will be a list of simulated measurements between satellites, representing what the VBAFDS software would accept from actual hardware sensors and inter-satellite communications links. Finally, based upon validation of the measurement models and this dynamic simulation environment, performance estimates will be generated which will quantify the effectiveness of VBAFDS for different missions and scenarios.

A reliable method for unique visual identification of satellites—perhaps based on synchronization between beacon illumination and imaging—is also yet to be formalized.

As small-spacecraft become ever more capable, formation flight systems will become increasingly feasible and attractive. Consequently, a technology such as VBAFDS, which facilitates distributed fleet operations by enabling coordinated navigation without substantial increases in complexity or bus resources, will prove highly beneficial to those communities seeking to leverage the powerful advantages of formation sytstems. Among the many applications to future government, civil, and commerical space missions, NASA has several strong candidate programs, including: the 10+ spacecraft Solar Flotilla heliospheric observation formation; the four-spacecraft Magnetospheric Multiscale formation which will study magnetosphere dynamics, the two-spacecraft X-Ray astronomy mission Constellation-X, and Stellar Imager.

While Earth science and military initiatives have thus far provided the most enthusiastic support for the formation concept, the programmatic capabilities unique to multiple-spacecraft platforms are equally valid for commercial operators as distribution of assets decreases single-event risk and facilitates system upgrade through replacement of individual elements. VBAFDS will enable the low-cost deployment of these system by reducing both the required platform resources (e.g., mass and power) and operational burden associated with their deployment. These benefits are of paramount concern to for-profit enterprises and could enable the advancement of a number of them, including remote sensing, geo-location, and sparse aperture communications.

CONCLUSIONS

The Vision-Based Attitude and Formation Determination System will offer a valuable integrated GN&C technology for future formation flight missions. Synthesizing a minimal set of measurement data that may be limited to as much as a single range value and bearing angle data, VBAFDS will enable the complete determination of formation geometries in both relative and inertial space. While capable of selectively drawing upon external resources such as GPS or ground-uplink, it is not constrained to their access or near-Earth operations. Design work conducted to date by AeroAstro has shown feasibility of the VBAFDS concept through determination of the key parameters and requirements necessary to proceed with development of test-prototype hardware and processing algorithms.

REFERENCES

1. NASA 2003 SBIR/STTR Solicitations, http://sbir.gsfc.nasa.gov/SBIR/sbirsttr2003/solicitation/index.html

2. Zenick, R. and McGuire, T., *Lightweight, Low-Power Coarse Star Tracker*, SSC03-X-7, AIAA/USU Conference on Small Satellites, Logan, Utah, August 11-14th, 2003.

3. IBIS4 SXGA Image Sensor Datasheet, Fillfactory, http://www.fillfactory.com/.

4. LED Datasheet, Agilent Technologies, http://we.home.agilent.com/.

5. Standard Laser Module VM63505 (class IIIa) Datasheet, Midwest Laser, http://www.midwest-laser.com/html/laser_diode_modules.html

6. STARNav Project, Texas A&M University, http://jungfrau.tamu.edu/%7Ehtml/StarNav/home.html

7. Samaan, M and Junkins, J. *Lost-in-space pyramid algorithm for robust star pattern recognition*, American Astronautical Society Guidance and Control Conference, 2001.

6. Wolf, Paul R. and Ghilani, Charles D., *Adjustment Computations, Statistics and Least-squares in Surveying and GIS*, Wiley Series in Surveying and Boundary Control, 1997

7. Triggs, Bill et. al, *Bundle Adjustment --- A Modern Synthesis,* To appear in Vision Algorithms: Theory & Practice. Springer-Verlag, 2000

8. Brown, Robert G. and Hwang, Patrick Y.C., *Introduction to Random Signals and Applied Kalman Filtering*, John Wiley and Sons, New York, NY, 1997.

9. Stengel, Robert F., *Optimal Control and Estimation*, Dover Publications, Inc, New York, NY, 1994.

10. Shinners, Stanley M., *Modern Control System Theory and Application*, Addison-Wesley Publishing Company, Reading, MA, 1972.

11. Gelb, Arthur (editor), *Applied Optimal Estimation*, MIT Press, Cambridge, MA, 1974.

12. S.P. Airey, G. Berrighi, and D. Procopio. "Seeing Through Dust Tracking Stars from within a Cometary Dust Cloud." American Astronautical Society, (AAS 03-022), 2003

13. Alfriend, K., "Dynamics and Control of Formation Flying Satellites," Invited Talk, Massachusetts Institute of Technology, Cambridge, MA, March 2004.

14. Carpenter, J., Leitner, J., Folta, D., Burns, R., "Benchmark Problems for Spacecraft Formation Flying Missions," AIAA Paper 2003-5364, August 2003.

15. Sabol, C., Burns, R., and McLaughlin, C., "Satellite Formation Flying Design and Evolution," *Journal of Spacecraft and Rockets*, Vol.38, No.2, 2001, pp.270-278.

16. The Lua programming language, http://www.lua.org/